Applied Thermal Engineering 165 (2020) 114566

Contents lists available at ScienceDirect

Applied Thermal Engineering

journal homepage: www.elsevier.com/locate/apthermeng

A novel methodology for Rankine cycle analysis with generic heat exchanger models

Brede A.L. Hagen[a,*], Monika Nikolaisen[b], Trond Andresen[b]

[a] Department of Energy- and Process Engineering, NTNU – Norwegian University of Science and Technology, Kolbjørn Hejes vei 1B, NO-7491 Trondheim, Norway
[b] SINTEF Energy Research, Sem Sælands vei 11, 7034 Trondheim, Norway

HIGHLIGHTS

- A new methodology based on a generic heat exchanger model is proposed.
- This methodology is a more informative alternative to pure thermodynamic analyses.
- Optimize the trade-off between heat transfer coefficient and pressure drop.
- Optimal heat exchanger design depends on its allowed size and the working fluid.
- The new methodology can be applied to both design and off-design analysis.

ARTICLE INFO

Keywords:
Rankine cycle
ORC
Generic heat exchanger
Modelling
Optimisation

ABSTRACT

This study presents a novel approach for Rankine cycle (RC) analysis, introducing a generic counter current heat exchanger (HX) model to enable basic fluid thermal and flow behaviour in HXs to be considered in a cycle optimisation process. The generic HX model does not represent a certain HX-type or even a manufacturable design, but applies fluid properties and a minimum amount of generic geometry parameters to estimate local heat transfer coefficients and pressure gradients. The proposed methodology thus permits simultaneous optimization of process state points and the trade-off between overall heat transfer coefficient and pressure drop without relying on a specific HX-geometry concept. The proposed methodology is demonstrated for evaluation of single-stage recuperated RC's of different HX size and working fluids, and compared with more conventional thermodynamic analyses. The comparison showed that the novel analysis resulted in lower net power output than the thermodynamic analyses due to working fluid-depending pressure drop in heat exchangers, and a quantitative HX size estimate in terms of total HX area based on working-fluid depended heat transfer coefficients. We therefore suggest the novel analysis as a low effort and more informative alternative to pure thermodynamic approaches for initial RC analyses.

1. Introduction

The Rankine cycle (RC), conventionally referred to as ORC when it employs an organic working fluid, is a mature technology. It can be applied to for instance power production from industrial waste heat and from renewable energy sources such as geothermal energy, biomass and solar energy [1]. However, the full potential of RCs is far from reached as the power production potential from the above-mentioned energy sources alone could meet the worlds power demand [2]. One step towards increasing the utilization of RCs, and thus facilitate reduction of greenhouse gas emissions from fossil fuel power plants, is to optimise the RC for each application. This is a challenging task and research efforts on RCs typically focus on certain aspects such as application, expander technology, dynamics, working fluid, cycle architecture or optimization [3]. This paper focuses on the underlying methodology of the three last aspects, hereafter referred to as RC analysis.

Rankine cycle analysis can be classified into two approaches (thermodynamic and thermo-economic) [4], defined and exemplified in the following sections. A thermodynamic analysis consists of determining optimal operating conditions for a set of working fluid candidates or cycle layouts subjected to thermodynamic objective function(s) and constraints. A common assumption in these analyses is fixed pinch point temperature differences (PPTDs) in the heat exchangers (HXs), hereafter referred to as “PPTD analysis” [5–7].

* Corresponding author.
E-mail address: brede.hagen@ntnu.no (B.A.L. Hagen).

https://doi.org/10.1016/j.applthermaleng.2019.114566
Received 14 March 2019; Received in revised form 2 October 2019; Accepted 19 October 2019
Available online 21 October 2019

Nomenclature

A	HX surface area, m^2
A_{cross}	Flow cross-sectional area m^2
D	Hydraulic diameter, m
f	Friction factor
h	Specific enthalpy, J/kg
i	Integration step index
k	Thermal conductivity, W/mK
L	HX flow length, m
$\dot{m}$	Mass flow, kg/s
M	Molar mass, g/mol
n	Number of integration steps
p	Pressure, kPa
Δp	Pressure loss, Pa
P	Channel perimeter, m
Q	Heat transfer rate, W
R	Thermal resistance, mK/W
T	Temperature, K
$\Delta\bar{T}$	Mean temperature difference, K
U	Overall heat transfer coefficient, W/m^2K
UA	Product of overall HTC and HX area, W/K
v	Fluid velocity, m/s
W	Electric power, W
x	Position in HX flow direction, m, vapor quality

Greek symbols

α	Local heat transfer coefficient, W/m^2K
ρ	Fluid mass density, kg/m^3
η	Efficiency

Subscripts

1–11	State points in the cycle (Fig. 3)
c	Cold side
cond	Condenser
evap	Evaporator
exp	Expander
gen	Generator
h	Hot side
is	Isentropic
m	Motor
pump	Pump
recup	Recuperator
s	Heat sink
spec	Specification
tot	Total
w	HX channel wall
wf	Working fluid

Acronyms

GHX	Generic heat exchanger
HTC	Heat transfer coefficient
HX	Heat exchanger
LMTD	Log mean temperature difference
NPV	Net present value
ORC	Organic Rankine cycle
PPTD	Pinch point temperature difference
RC	Rankine cycle

PPTD analysis is often used for comparison of different RCs that operate under the same boundary conditions. For instance, previous PPTD analyses have demonstrated that the transcritical cycle has a better thermodynamic performance potential than the subcritical cycle [8–10]. Chys et al. [7] used a PPTD analysis to demonstrate up to 16% increase in thermodynamic performance by using zeotropic mixtures instead of pure working fluids. Wu et al. [11] confirmed the superior thermodynamic performance potential of zeotropic mixtures, but demonstrated that the ratio between net power output and the total HX UA-value decreased, indicating that improved performance with zeotropic mixtures comes at the cost of larger heat exchangers. PPTD analysis has also been applied to compare the subcritical cycle with the trilateral flash cycle [12] and for working fluid screening of RCs utilizing LNG cold energy [13]. Vivian et al. [14] performed a PPTD analysis of multiple working fluids for both recuperated and non-recuperated cycles. They demonstrated that for a heat source inlet temperature of 180 °C, adding a recuperator can give up to 9% increase in thermodynamic performance when the there is a lower limit on the heat source outlet temperature.

The main advantage of PPTD analysis is that it is fast and only requires PPTDs for defining the HXs. However, ranking a set of working fluids, cycle layouts or optimum operating conditions (i.e. subcritical vs. transcritical) from best to worst with a PPTD analysis alone is challenging, since heat exchangers of equal PPTDs does not necessarily correspond to equal HX sizes, costs, or fluid pressure drop. In addition, as several authors have pointed out, there is a trade-off between HX size and net power output when selecting PPTDs in the HXs [15–17], and the optimal values of PPTDs in each heat exchanger are not obvious [18].

Thermodynamic analysis can partly overcome the above-mentioned issues by optimizing the PPTD's in the heat exchangers with a constraint on the total HX UA-value, hereafter denoted UA-analysis. To the best of our knowledge, UA-analysis is rarely performed; the most relevant publication found was Ref. [19] where different CO_2 Brayton cycles with identical total UA-values were compared. A similar methodology was employed in Ref. [20], where total HX area (based on predefined values for overall HTC) was used as a basis for comparison between working fluids for both subcritical RC and the trilateral flash cycle. However, it has been stressed that UA-value is only a preliminary indicator of HX size due to its approximation of equal heat transfer coefficients [21].

Thermo-economic analyses include cost estimates, in addition to the thermodynamic performance, in the objective function or constraints. Thermo-economic analyses can therefore search for the optimal compromise between system cost and thermodynamic performance. One example is the study by Walraven et al. [22], who analysed RCs of different configurations and working fluids for geothermal heat sources. The authors used an air-cooled condenser model and a shell and tube model for the remaining heat exchangers. They simultaneously optimised process conditions and HX geometry parameters to maximize the net present value (NPV) of the installation, assuming a lifetime of 30 years. They found that the heat source inlet and outlet temperatures, as well as economic parameters such as electricity price and discount rate, had a strong influence on the NPV. The work illustrates that thermo-economic analysis gives detailed results but requires a larger amount of uncertain, application dependent input parameters compared to the thermodynamic analyses.

Other examples of thermo-economic studies are found in Refs. [23–25]. All these studies consider at least three working-fluid candidates, involve detailed heat exchanger models and both thermodynamic and economic performance are included in the objective function. The results from Refs. [24,25] did not show any economic advantage of using zeotropic mixtures instead of pure working fluids even though thermodynamic analyses has proven superior thermodynamic

performance potential of zeotropic mixtures [7]. A comparison between thermodynamic- and thermo-economic analysis was performed by Quoilin et al. [26] for working fluid selection of a small-scale RC for waste heat application. Their results demonstrated that the two methodologies gave different results in the ranking of the working fluid candidates from best to worst, as well as different evaporation temperature. The paper concludes that thermodynamic analysis may not identify the best working fluid in terms of economic profitability.

Thermo-economic analyses have also been applied for RC-optimization considering off-design performance [27,28]. Results in Ref. [28] demonstrated that the most economic design compensated slightly undersized heat exchangers and turbines, with good performance at off-design conditions. Although this approach is very promising for a realistic design optimisation, additional requirements for such analyses are the knowledge of the variations in the boundary conditions with time, and part-load models for the components.

Thermo-economic analyses provide quantitative results but are very specific and thus challenging to apply for an application where for instance the optimal set of component types are unknown. Furthermore, thermo-economic analyses are also computationally demanding for cases with multiple working fluid or cycle layout candidates. In such cases, the number of candidates can be reduced by using an initial screening analysis. Thermodynamic analysis is the traditional method for screening multiple working fluid candidates. However, the above-mentioned studies indicate that thermodynamic analysis might give misleading results, partly because the heat transfer coefficient depends on the working fluid, which is particularly true for two-phase flow of pure fluids vs. zeotropic mixtures, or for boiling vs. supercritical heating.

Using thermal-hydraulic heat exchanger models in the system optimization (without considering cost) is one way of obtaining realistic estimates of HX design and size. One example is the study by Dong et al. [29], who performed a PPTD analysis of pure and zeotropic working fluids mixtures followed by a heat exchanger area calculation based on concentric double pipe HXs with fixed diameters. The analysis showed that zeotropic mixtures increased net power production under the fixed PPTD assumption, but the ratio between net power production and total HX area was reduced. Walraven et al. [30] optimized Rankine Cycles of different pure working fluids and layouts considering both shell-and-tube and plate HX. They demonstrated that systems with plate HXs perform better that systems with shell and tube HXs. They also pointed out that a possible disadvantage of plate HX with equal number of fluid passes is that the fluid channels are of equal cross-sectional area, which might lead to an inefficient heat exchanger if the volume flow rate of the two fluids differ significantly. These studies solve the problem of determining realistic estimates of HX size, but still they rely on a predefined HX geometry concept.

With basis in existing literature on we believe there is a need for a new, low computationally demanding approach to RC analysis that gives more informative results than the thermodynamic analyses, without the need for pre-selecting component types. The novel methodology for RC analysis presented in this paper is a step towards such an approach and involves the use of a generic thermal-hydraulic HX model, hereafter referred to as the GHX-model. The idea of a generic HX model is not completely new. Some of the HX's in Refs. [31,32] were modelled by stacked layers of multiport tubes to represent a generic compact heat exchanger. However, this work takes this approach a step further since the GHX-model does not represent any manufacturable HX design. Instead, the HX geometry is defined by the generic geometry parameters required for applying thermal-hydraulic correlations for channel flow. This novel approach permits simultaneous optimization of process state points and the trade-off between overall heat transfer coefficient and pressure drop in the HX's. As such, this approach includes the effect of pressure drop on the net power output and provides a quantitative basis for HX size comparison in terms of total HX area. The proposed methodology thus permits comparison of different RCs of equal total HX area, without having to decide which specific HX types to use.

The paper is organised as follows: the proposed RC model and optimisation formulation is presented in detail in Section 2. Section 3 demonstrates the novel methodology by analysing Rankine cycles with different working fluids and HX sizes for a given heat source. The simulation results from the novel methodology are compared with results from the two thermodynamic analyses described. The most important results are discussed in Section 4, and conclusions drawn from this study are given in Section 5.

2. Methodology

2.1. The novel Rankine cycle analysis

The novel Rankine cycle analysis, hereafter denoted “GHX-analysis”, involves the use of a generic heat exchanger model (GHX-model), the development of a RC model that applies the GHX-model, and an optimisation formulation. These three elements are described in detail in the following three subsections.

2.1.1. The GHX-model

The GHX-model involves a somewhat abstract representation of heat transfer mechanisms, and does not require specification of heat exchanger type, i.e. shell and tube, plate or finned tube, etc. Only five generic HX parameters are required to specify the HX geometry; hydraulic diameter (both fluids), flow cross-sectional area (both fluids) and length (the same for both fluids).

These geometry parameters provide the information required to apply thermal-hydraulic correlations for heat transfer and pressure drop. Fig. 1 shows an example cross-section of the GHX-model under the assumption that the fluids flow in multiple circular channels. In this example the hydraulic diameter is the channel diameter and the cross-sectional flow area on the hot and cold side is represented by the red and blue areas, respectively.

The remainder of this section contains a detailed mathematical description of the GHX-model, which consists of three differential equations that have to be solved. The first differential equation (Eq. (1)) describes the heat transfer rate per unit length between the hot and cold fluids.

$$\frac{dQ}{dx} = \frac{T_h - T_c}{R} \tag{1}$$

The total thermal resistance between the hot and cold fluids, R,

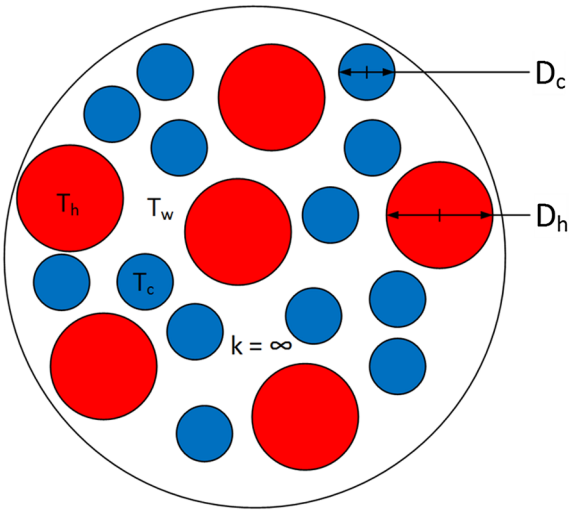

Fig. 1. Example cross-section of the generic HX model under the assumptions that the fluids flow in multiple circular channels.

Table 1
Heat transfer and pressure drop correlations employed in the GHX-model.

Flow	Heat transfer	Pressure drop
Single-phase	Gnielinski [33]	Selander [34]
Two-phase	Boyko and Kruhzilin [35] (condensation) Bennet & Chen [36] (evaporation) Silver [37] and Bell and Ghaly [38] for the mixture effects in multicomponent condensation and evaporation	Friedel [39] with single-phase formulation by Selander [34]

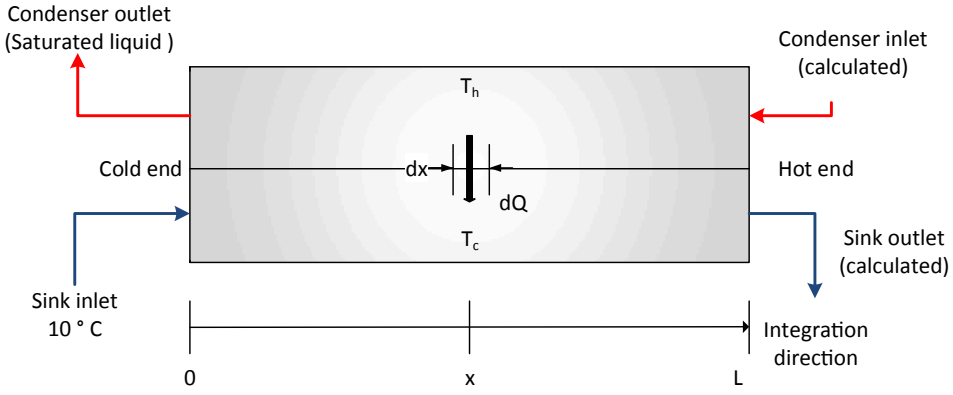

Fig. 2. Calculation of the condenser using the GHX-model.

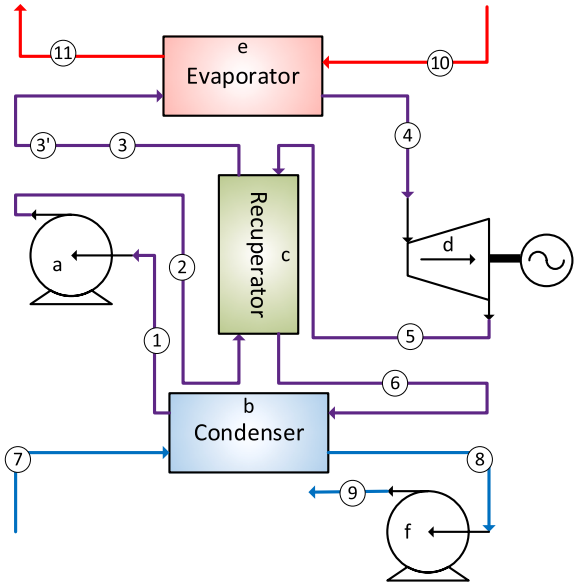

Fig. 3. The single-stage recuperated RC. Letters a-f indicate the component calculation sequence for the novel RC model using generic HX models. Numbers 1–11 indicate the state points (pressure and enthalpy) in the RC model.

includes thermal resistance from convection according to Eq. (2).

$$R = \frac{1}{\alpha_c P_c} + \frac{1}{\alpha_h P_h},\ P = \frac{4A_{cross}}{D} \tag{2}$$

The two remaining differential equations calculate the change in pressure per unit length of the hot and the cold fluids in the HX:

$$\frac{dp_j}{dx} = \pm f_j \frac{\rho_j v_j^2}{2D_j},\ j = c,\ h \tag{3}$$

The ± symbol in Eq. (3) indicates that pressure can either increase or decrease when integrating through the HX since the fluids flow in opposite directions.

Heat transfer coefficients and friction factors can either be set to constant values or calculated by thermal hydraulic correlations taking into account transport-properties such thermal conductivity and viscosity. There are multiple thermal-hydraulic correlations available for channel flow and the discussion of the optimal set of correlations are

Table 2
Optimization formulation for the three different analyses considered in this paper. In each column below the headings indicating the analysis type, "X" means that the variable or constraint is applied, while "-" means that it is not applied.

		Analysis method		
	Variable/Function	GHX	UA	PPTD
Process variables	p_1	X	X	X
	p_2	X	-	-
	p_4	X	X	X
	h_4	-	X	X
	$\dot{m}_{wf}$	X	X	X
	$\dot{m}_s$	X	X	X
	Q_{recup}	–	X	X
Evaporator geometry variables	L	X	–	–
	$A_{cross,wf}$	X	–	–
Condenser geometry variables	L	X	–	–
	$A_{cross,wf}$	X	–	–
Recuperator geometry variables	L	X	–	–
	$A_{cross,h}$	X	–	–
	$A_{cross,c}$	X	–	–
Equality constraints	$p_3 - p_{3'} = 0$	X	–	–
	$h_3 - h_{3'} = 0$	X	–	–
Inequality constraints	$T_{11} - T_{11,spec} \geq 0$	X	X	X
	$x_4 - 1 \geq 0$	X	X	X
	$x_5 - 1 \geq 0$	X	X	X
	$A_{tot,spec} - A_{tot} \geq 0$	X	–	–
	$UA_{tot,spec} - UA_{tot} \geq 0$	–	X	–
	$PPTD_{spec} - PPTD_{recup} \geq 0$	–	–	X
	$PPTD_{spec} - PPTD_{cond} \geq 0$	–	–	X
	$PPTD_{spec} - PPTD_{evap} \geq 0$	–	–	X
Objective function	W_{net}	X	X	X

Table 3
Heat source and heat sink parameters in simulation case.

	Case parameters	Unit	
Heat source	Fluid	–	Water
	Inlet temperature	[°C]	140
	Lower temperature limit (inequality constraint)	[°C]	70
	Mass flow	[kg/s]	2.9
	Pressure	[bar]	10
Heat sink	Fluid	–	Water
	Inlet temperature	[°C]	10

Table 4
Fixed parameters for the demonstration cases. Parameters for expander and pump are employed in both the thermodynamic and the novel GHX-analysis, while the HX parameters are only relevant for the GHX-analysis.

Component	Parameter	Unit	Value
Pumps	Isentropic efficiency	–	0.70
	Motor efficiency	–	0.95
Expander	Isentropic efficiency	–	0.85
	Generator efficiency	–	0.95
Evaporator	Hydraulic diameter, working-fluid side	[cm]	1.0
	HTC heat-source side	[kW/m^{2}K]	5.0
	Heat-source pressure drop	[kPa]	0.0
	Area ratio (hot/side)	–	1.0
Condenser	Hydraulic diameter, working-fluid side	[cm]	2.0
	Hydraulic diameter, sink side	[cm]	2.0
	Sink side cross-sectional area	[cm^2]	100
Recuperator	Hydraulic diameter, low-pressure side	[cm]	2.0
	Hydraulic diameter, high-pressure side	[cm]	1.0

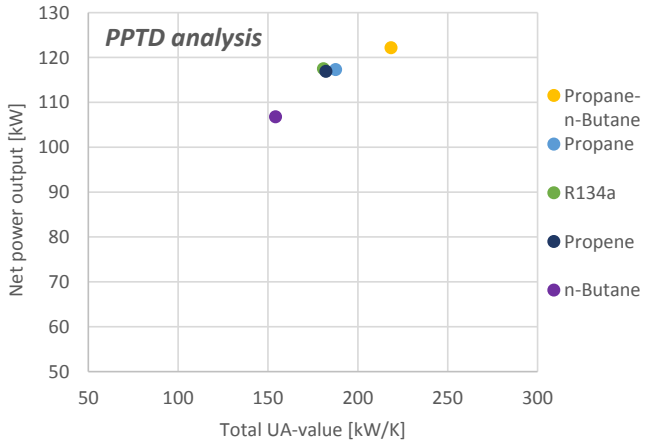

Fig. 4. Results of the PPTD analysis, showing maximized net power versus total UA-value for the different working fluids.

out of the scope of this article. The correlations applied in this work are widely used and based on experiments of flow in circular channels and cover both single-phase and two-phase flow of mixtures and pure fluids, Table 1. We believe that the chosen correlations are adequate for generic heat exchanger analysis, because they are mainly functions of physical properties and the Reynolds number and involves a minimum of regression coefficients. Therefore, these correlations are relatively safe with respect to extrapolation to fluids not being subjected to experimental activity during the correlation development.

The GHX-model requires the fluid states at either the hot or the cold end to be specified. These states are the *boundary conditions* for Eq. (1) and Eq. (3).

A calculation example for the condenser is presented, and calculations of the other HXs are similar. In the condenser, the states at the

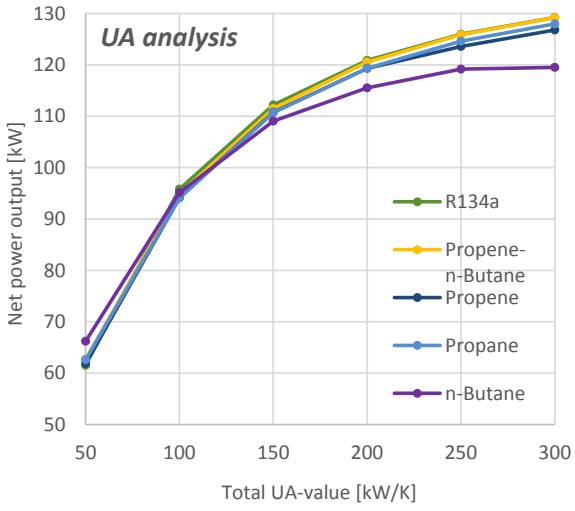

Fig. 5. Results of the UA-analysis, showing maximised net power versus total UA-value for the different working fluids.

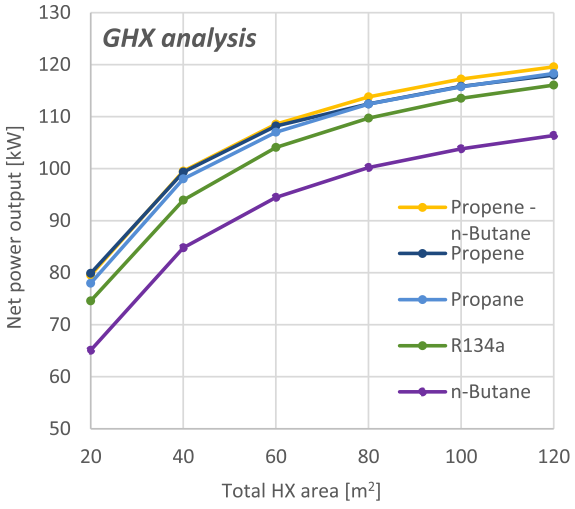

Fig. 6. Results of the GHX-analysis, showing maximized net power versus total HX area for the different working fluids.

cold end are specified, Fig. 2. The condenser is solved by n equidistant numerical integration steps, starting at the cold end. Eq. (1) is solved by a fourth-order Runge-Kutta method and gives the fluid enthalpies for the next step. Eq. (3) is solved by an explicit Euler method and gives the fluid pressures for the next step. Outputs from the GHX-model are the heat duty, HX area, pressure drop of both fluids and an estimate of the overall heat transfer coefficient $U = \frac{Q}{A\Delta\bar{T}}$, where $\Delta\bar{T} = \frac{1}{L}\int_0^L \Delta T dx$ is the mean temperature difference between the hot and cold fluids, and is approximated by the trapezoidal method for numerical integration, Eq. (4).

$$\Delta\bar{T} = \frac{1}{n}\sum_{i=1}^{n}\frac{\Delta T_i + \Delta T_{i-1}}{2} \tag{4}$$

The HX area for the condenser and evaporator, $A_{cond,evap} = P_{wf}L$, is calculated as the surface area on the working-fluid side, while the recuperator area $A_{recup} = \frac{1}{2}(P_c + P_h)L_{recup}$ is calculated as the average value of the surface area on the high- and low-temperature sides of the recuperator.

2.1.2. The Rankine cycle model

A graphical illustration of the RC model is shown in Fig. 3, which represents the well-known single-stage recuperated RC. The non-

Table 5
Optimisation results from GHX-analysis with maximum total HX area of 60 m^2.

Working fluid		Propene/n-Butane	Propene	Propane	R134a	n-Butane
Net power	[kW]	108.5	108.2	107.0	104.1	94.5
Process parameters						
Pump inlet pressure	[bar]	9.6	10.6	8.6	6.3	2.5
Expander inlet pressure	[bar]	49.1	51.6	46.6	43.6	14.0
Working fluid mass flow	[kg/s]	2.0	2.0	2.0	3.8	1.9
Heat sink mass flow	[kg/s]	24.0	25.8	25.8	25.2	26.8
Evaporator						
Length	[m]	37.5	35.8	38.3	35.9	26.0
$A_{cross,wf}$	[cm^2]	19.1	19.9	18.7	19.5	25.8
Area	[m^2]	28.7	28.4	28.6	27.9	26.8
Heat duty	[kW]	860	862	862	862	862
Overall HTC	[W/m^2K]	2881	2853	2887	2730	2376
Working fluid pressure drop	[kPa]	148	148	153	194	77
PPTD	[K]	4.9	4.6	4.8	4.9	2.6
Condenser						
Length	[m]	29.2	29.3	29.7	23.4	17.5
$A_{cross,wf}$	[cm^2]	43.9	43.0	44.0	59.4	95.2
Area	[m^2]	25.6	25.2	26.1	27.8	33.3
Heat duty	[kW]	740	742	743	748	757
Overall HTC	[W/m^2K]	3047	3206	3052	2390	1638
Working fluid pressure drop	[kPa]	75	79	85	82	31
Heat sink pressure drop	[kPa]	90	103	104	79	66
PPTD	[K]	8.4	7.1	7.3	9.1	11.2
Recuperator						
Length	[m]	6.0	6.9	5.5	3.4	0.0
$A_{cross,h}$	[cm^2]	71.6	69.9	74.5	98.8	–
$A_{cross,c}$	[cm^2]	11.3	11.1	11.0	13.8	–
Area	[m^2]	5.7	6.4	5.3	4.3	–
Heat duty	[kW]	82	87	85	51	–
Overall HTC	[W/m^2K]	1012	1064	1024	745	–
Cold-side pressure drop	[kPa]	31.3	38.6	31.0	19.1	–
Hot-side pressure drop	[kPa]	8.3	9.6	7.6	5.7	–
PPTD	[K]	11.5	10.0	13.0	14.0	–
Optimization constraint						
Total HX area	[m^2]	60.0	60.0	60.0	60.0	60.0

recuperated cycle can also be analysed by the RC model by setting the recuperator length to zero. This means that when the recuperator length is a free optimisation variable, both non-recuperated and recuperated RC configurations are considered.

Numbers 1–11 in Fig. 3 represent the state points in the RC model and are defined by pressure and enthalpy. The thermodynamic properties and the transport properties were calculated using the NIST Standard Reference Database, Refprop version 9.1 [40].

Models for the expander and pumps require the inlet state and outlet pressure to be specified and are modelled with constant isentropic and mechanical efficiencies according to Eqs. (5) and (6).

Pump model:

$$\eta_{is} = \frac{h(p_{out}, s_{in}) - h_{in}}{h_{out} - h_{in}}$$

$$W_{pump} = \frac{1}{\eta_m}\dot{m}(h_{out} - h_{in}) \quad (5)$$

Expander model:

$$\eta_{is} = \frac{h_{in} - h_{out}}{h_{in} - h(p_{out}, s_{in})}$$

$$W_{exp} = \eta_{gen}\dot{m}(h_{in} - h_{out}) \quad (6)$$

The letters a-f in Fig. 3 indicate the component calculation sequence. Saturated liquid at state point 1 enters the pump and state point 2 is calculated with the pump model using the specified pump outlet pressure. The condenser is then solved from the cold to the hot end (as described in Section 2.1.1) and state points 6 and 8 are calculated. The state points at the cold end of the recuperator are thus defined, which is the next component to be solved, and state points 3 and 5 are calculated. The expander model is thereafter solved iteratively to find the expander inlet enthalpy using the specified expander inlet pressure and state point 5. Then the evaporator is solved from the hot to the cold end and state points 3′ and 11 are calculated. Finally, the heat sink pump is calculated with a pressure lift equal to the heat sink pressure drop in the condenser, such that the pressures at state points 7 and 9 are equal.

2.1.3. Rankine cycle optimisation

The purpose of the Rankine cycle optimisation is to find the optimal HX geometry and process design that maximizes the net power output (Eq. (7)), subject to a set of constraints that will guarantee a feasible process design.

$$W_{net} = W_{exp} - W_{pump,wf} - W_{pump,s} \quad (7)$$

The optimisation is performed using a gradient-based constrained optimisation solver, NLPQL[41]. The variables, constraint- and objective function for the optimisations are shown in Table 2. Note that expander inlet pressure is a free optimisation variable, which means that the solver can choose between subcritical and transcritical process designs.

Two equality constraints are imposed to ensure that the pressure and temperature at state points 3 and 3′ are identical. Two inequality constraints requiring dry vapour at expander inlet and outlet are also included. Hence, wet expansion cycles are excluded from this analysis. Without constraints on the HX size, the PPTDs in all heat exchangers will be infinitesimally small and the required HX area will increase towards infinity. A constraint on the maximum total HX area is

Table 6
Optimized process and HX geometry from the GHX-analysis for propene.

Total HX area	[m^2]	20	40	60	80	100	120
Net power	[kW]	79.9	99.5	108.2	112.4	115.8	118.0
Process parameters							
Pump inlet pressure	[bar]	11.6	11.0	10.6	10.8	10.7	10.6
Expander inlet pressure	[bar]	51.5	51.8	51.6	51.8	52.4	51.8
Working fluid mass flow	[kg/s]	2.1	2.0	2.0	2.0	2.0	2.1
Heat sink mass flow	[kg/s]	27.6	26.0	25.8	22.6	22.0	23.4
Evaporator							
Length	[m]	25.1	32.2	35.8	38.9	38.7	41.9
$A_{cross,wf}$	[cm^2]	11.8	16.3	19.9	20.6	27.9	27.0
Area	[m^2]	11.8	21.0	28.4	32.1	43.2	45.2
Heat duty	[kW]	845	860	862	862	862	862
Overall HTC	[W/m^2K]	3414	3060	2853	2824	2491	2496
Working fluid pressure drop	[kPa]	250	181	148	149	89	112
PPTD	[K]	13.8	7.8	4.6	3.3	1.6	1.4
Condenser							
Length	[m]	19.9	25.4	29.3	30.3	32.0	32.4
$A_{cross,wf}$	[cm^2]	20.6	32.5	43.0	65.6	67.8	81.6
Area	[m^2]	8.2	16.5	25.2	39.8	43.4	52.8
Heat duty	[kW]	755	749	742	738	735	732
Overall HTC	[W/m^2K]	6429	4028	3206	2159	2126	1837
Working fluid pressure drop	[kPa]	175	107	79	41	42	30
Heat sink pressure drop	[kPa]	80	91	103	83	84	95
PPTD	[K]	12.7	9.1	7.1	6.0	5.4	5.0
Recuperator							
Length	[m]	0.0	3.6	6.9	7.9	10.2	15.0
$A_{cross,h}$	[cm^2]	–	54.1	69.9	77.5	99.7	103.7
$A_{cross,c}$	[cm^2]	–	9.0	11.1	12.7	15.7	21.5
Area	[m^2]	–	2.6	6.4	8.1	13.4	22.0
Heat duty	[kW]	–	55	87	92	105	118
Overall HTC	[W/m^2K]	–	1334	1064	963	778	615
Cold-side pressure drop	[kPa]	–	29.4	38.6	34.6	30.5	25.0
Hot-side pressure drop	[kPa]	–	7.7	9.6	9.2	7.5	9.7
PPTD	[K]	–	14.0	10.0	8.6	6.7	4.1

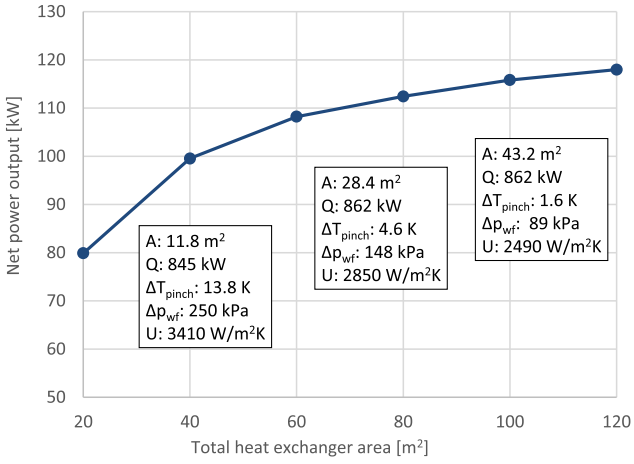

Fig. 7. GHX-analysis: Net power output with propene as working fluid, including selected optimisation results for the evaporator shown in data labels.

therefore imposed. In this case, the optimisation solver will search for the HX geometry that offers the best trade-off between overall HTC and pressure drop and the optimal HX area distribution between the three heat exchangers. In some cases, there are limitations on how far the heat source can be cooled down. We therefore imposed an optional constraint on the minimum heat source outlet temperature. Gradients of the objective function and the constraints were calculated using the second-order central difference approximation for numerical differentiation.

2.2. Thermodynamic analyses

The thermodynamic analyses presented in this work (referred to as PPTD- and UA-analysis) were performed by using a pure thermodynamic Rankine cycle model representing the same cycle layout as in Fig. 3. The thermodynamic model differs from the novel RC model only by using thermodynamic HX models. This HX model neglects working fluid pressure drop and calculates the UA-value and PPTD for given inlet and outlet states by discretising the HX into n sub-HXs of equal heat duty $Q_i = \frac{Q}{n}$. The UA-value was calculated as the sum of the UA-values of all n sub-HXs by the LMTD method given in Eq. (8).

$$UA = \sum_{i=1}^{n} \frac{Q_i}{LMTD_i} \tag{8}$$

The calculated PPTD is the smallest temperature difference between the hot and the cold fluid in all of the sub-HXs. The optimisation procedure for thermodynamic analyses resembles the procedure for the GHX-analysis described in Section 2.1.2, and is shown in detail in Table 2. The main difference is that the HX geometry variables are replaced by variables for expander inlet enthalpy and recuperator duty in order to have the same degrees of freedom on the process-variables as in the GHX-analysis. In addition, since pressure drop is neglected, the working fluid pump outlet pressure and expander inlet pressure refer to the same variable. The last difference in the optimisation procedure is the constraint on HX size. The PPTD analysis has three inequality constraints for minimum PPTDs of 5 K in each heat exchanger, while the UA-analysis has a constraint on the total UA-value in the HXs.

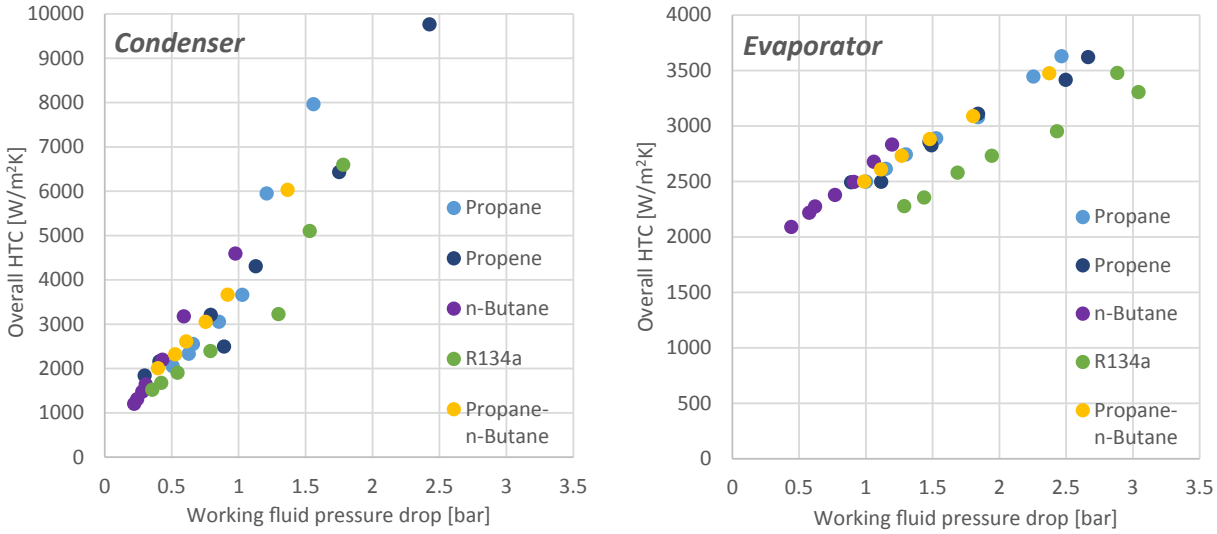

Fig. 8. Overall HTCs and working fluid pressure drops in optimised HXs from the GHX-analysis for different working fluids and total permitted HX area.

3. Demonstration of the novel Rankine cycle analysis

3.1. Description of simulation case

We have defined a simulation case, Table 3, to demonstrate the novel methodology. The case considers pressurised water at 140 °C as the heat source, with a constrained minimum temperature of 70 °C.

3.2. Fixed parameters

The fixed parameters for the optimisations performed in this work are shown in Table 4. Parameters for the expander and pumps are applied for both the thermodynamic and the novel GHX-analysis, while the remaining parameters are only relevant for the GHX-analysis.

To limit the number of free optimisation variables in the GHX-analysis, but at the same time enable optimizing the trade-off between overall HTC and pressure drop, the hydraulic diameters in the heat exchangers are kept constant. Their values might not be the optimal one from a thermal-hydraulic point of view. However, the fixed values at least ensure that the hydraulic diameter are within a reasonable size with respect to for instance validity of the thermal-hydraulic correlations. We also assumed that the high-pressure channels (working fluid side of evaporator and high-pressure side of recuperator) prefer a lower hydraulic diameter than the remaining channels. In addition, the cross-sectional flow area of the sink channel in the condenser was fixed to 100 cm^2. This resulted in a heat sink velocity of 2–3 m/s.

The evaporator calculation is somewhat simplified, as there is no geometry-based calculation on the heat source side. Instead, the heat-source pressure drop is neglected, a fixed heat transfer coefficient is assumed on the heat source side, and an area ratio of unity is set. The reason for this simplification is to reduce the number of free optimisation variables and thus model complexity, but also to avoid having to describe an objective function penalty caused by pressure loss in the heat source fluid, which is regarded here as being part of an industrial process. Geometry-based calculations of the heat-sink side of the condenser were included in the demonstration of the GHX-analysis, and the heat-sink pressure drop relates directly to the sink pump work.

3.3. Working fluids

International legislation, such as the Montreal and the Kyoto Protocols, place restrictions on the use of certain working fluids, and call for a shift from artificial refrigerants towards natural working fluids with low global-warming and ozone-depletion potential [21]. Hence, the natural propene, propane and n-Butane are selected for the demonstration of the GHX-analysis, in addition to the conventional refrigerant R134a as a baseline.

A mixture of 94.1 mol percent propene and 5.9 mol percent n-Butane was included to provide comparison between pure working fluids and a mixture. For simplicity, the composition of the mixture was optimised for a total UA-value of 150 kW/K and was used throughout the UA- and GHX-analysis.

3.4. Simulation results

The main results of the PPTD-, UA-, and GHX-analysis are shown in Fig. 4-Fig. 6, respectively. In the PPTD analysis, maximized net power output was plotted against total UA-value for the different working fluids; the UA-value was calculated based on the results of the cycle optimisation.Fig. 5.

The results of the UA-analysis are shown on the same axis, but power output has been optimised for a range of equal total UA-values, resulting in a “performance landscape” showing how the working fluids compare across a range of total UA-values, indicating the total size of the heat exchangers. The simulation points from the PPTD analysis are not necessarily located on the curves from the UA-analysis, since optimal PPTD's in the HXs could be different from the 5 K used in the PPTD analysis. Finally, results from the GHX-analysis are presented in a similar form to the UA-analysis, but note that net power is plotted against total HX area instead of total UA-value. The optimised n-Butane cycle is subcritical, and the remaining cycles are transcritical in all analyses.

In the PPTD analysis the mixture results in the highest net power, but simultaneously requires the largest UA-values. This illustrates that equal PPTD does not translate to equal UA or other expressions of HX size. The UA-analysis shows that all fluids achieve fairly similar net power outputs when given the same total UA budget. The exception is that the subcritical fluid n-Butane is slightly better for low UA-values, but starts to fall behind the others for larger UA budgets.

The general level of net power output is lower in the GHX-analysis than the UA-analysis and the working fluids rank differently compared to the UA-analysis. For instance, R134a is no longer one of the fluids with highest net power, and n-Butane shows poorer performance compared to the UA-analysis. Furthermore, the relative difference in net power between the fluids increased from the UA to the GHX-analysis.

Table 5 shows detailed optimisation results for all working fluid candidates with a total HX area of 60 m^2. The table shows that n-Butane

produces the lowest net power, but the optimised process is simpler than for the other working fluids since the recuperator is eliminated (i.e. the optimized recuperator length is zero). The table also shows that the optimized HX geometry differs with respect to working fluid. In particular, the condenser and evaporator for n-Butane are shorter, but designed with larger cross-sectional area compared to the corresponding HXs' with other fluids, resulting in a lower pressure drop and overall HTCs.

Table 6 shows detailed optimisation results for propene subjected to different constraint values for total HX area. The table shows that the optimised process has a larger expander pressure ratio and net power production as total HX area increases. The table also shows that the HX design and the HX area distribution are highly dependent on the total permitted HX area. For a total HX area of 20 m^2, the recuperator is not prioritised at all, while in the other cases the recuperator area is around 10% of the total HX area. Obviously, HX size (length and flow area) increases with increasing total HX area. However, for larger total HX areas, the condenser and evaporator are designed with lower pressure drops and overall HTCs.

4. Discussion

The previous section showed simulation results from the novel GHX-analysis and traditional thermodynamic analyses. The PPTD analysis predicted the largest thermodynamic performance for transcritical cycles of pure fluids and the zeotropic mixture, but these cycles also had the largest total UA-value. This in agreement with the results from Refs. [11,21]. The UA-analysis compared RCs at equal total UA-values across a wide range of HX sizes, represented by total UA-values, and demonstrated that the optimal working fluid depends on the permitted HX size.

The contribution of this work is the novel GHX-analysis, based on generic HX models and simultaneous optimisation of overall HTC vs. pressure drop trade-off and process parameters. The results from the GHX-analysis demonstrated that the trans-critical R134a and the subcritical n-Butane cycle both were outperformed by the other options for the whole range of considered system sizes. In contrast, the thermodynamic analysis predicted a relatively better performance of the two solutions. The fact that the outcome of an analysis depends in the underlying methodology have already been confirmed by Quoilin et al. [26]. If this hypothetical demonstration case instead were an initial part of a system design procedure; the next step could be to exclude the R134a and n-Butane solutions and perform a thermo-economic analysis of the remaining promising solutions. In addition, the optimized HX parameters such as pressure drop, cross-sectional flow area and surface area ratio could be used to give a flying start on the HX design, with respect to geometric configuration, thermal-hydraulic design or HX type. Such information cannot be provided by a thermodynamic analysis alone. The GHX analysis also demonstrated that adding a recuperator is beneficial only when a sufficient large total HX area is permitted. This is a new criterion for the selection of recuperated vs. non-recuperated cycle since previous literature mentions a constrained outlet heat source temperature and a sufficient high heat source inlet temperature as the main criterions for adding a recuperator [10,14].

Fig. 7 shows selected results from the GHX-analysis for propene as working fluid. Evaporator duty, PPTD, working fluid pressure drop and overall HTC are given in data labels for total HX areas of 20 m^2, 60 m^2 and 100 m^2. The figure illustrates how the cycle optimisation effectively finds the best trade-off between different component and cycle losses subject to the active constraints. For the lowest total HX area, the optimisation chooses a fairly high pressure drop to obtain high overall HTC. In the trade-off between quantity (duty) and quality (temperature) of recovered energy, a small fraction of the available heat source is not captured. When the total HX area “budget” increases, a shift in both these trade-offs can be observed. Pressure drop and heat transfer coefficients decrease, and all the available heat in the heat source is recovered at higher exergy, as the average temperature differences are reduced, as reflected in decreasing PPTD.

The overall HTCs and working fluid pressure drops in the optimised condensers and evaporators from the GHX-analysis are shown in Fig. 8. The figure illustrates strong positive correlations between pressure drop and overall HTC in the evaporator and condenser when the total permitted HX area is changed, indicating that the optimal trade-off between heat transfer and pressure drop depends on the total permitted HX size.

Fig. 8 can also be used to understand the difference between the results of the UA- and GHX-analysis. The GHX-analysis includes exergy losses due to working fluid pressure drop, resulting in lower net power output compared to the UA-analysis, which neglects working fluid pressure drop. In addition, the GHX-analysis calculates the UA-value as the product of HX area and overall HTC. Hence, the RCs are not necessarily compared at equal total UA-values in the GHX-analysis, as is the case for the UA-analysis. Therefore, discrepancies between the results of the thermodynamic- and GHX-analyses are to be expected for fluids with different overall HTCs. As an example, consider the overall HTCs of R134a in Fig. 8. When the overall HTCs in the evaporator at equal total pressure drops are compared, all hydrocarbons have relatively similar values, which are larger than overall HTCs for R134a. R134a also has lower HTCs than the hydrocarbons in the condenser. This effect is the main reason why R134a (the best pure fluid from the UA-analysis) was outperformed by several hydrocarbons in the GHX-analysis.

A reason behind the poor performance of the n-Butane cycle is also indicated here. n-Butane had significantly lower operating pressures than the other fluids, and cycle performance is thus more sensitive to working fluid pressure drop. As shown in Table 5, the n-Butane evaporator and condenser were designed with larger cross-sectional area and shorter length compared to the other fluids. This results in a lower pressure drop and overall HTC for the butane heat exchangers as can be seen in Fig. 8.

The GHX-model represents an abstract heat exchanger that cannot be manufactured, which implicates that experimental verification of the GHX-model, other than experimental verification of the thermal-hydraulic correlations, is impossible. However, the optimised operating conditions and the pressure drops from the GHX-analysis could be applied as input for a HX type-specific design optimisation. In this case, the resulting heat transfer area from such an analysis could be compared with the HX area predicted by the GHX-model for evaluating the accuracy of the GHX-model with respect to estimating size of real heat exchangers. Whether the use of thermal-hydraulic correlations for circular channels are realistic for the final application, also depends on choice of HX technology at the later stage. However, the presented approach is based on the assumption that the trade-off between overall HTC and pressure is similar in nature across common HX types. Validation this assumption is suggested for future work.

The isentropic efficiency of the expander has a strong influence on the expander power and thereby the performance of the Rankine cycle. Further development of a generic RC analysis should therefore include a more detailed expander model capable of predicting performance based on fluid properties and operating conditions.

The accuracy of the optimisation in terms of finding the global optimal solution should also be discussed. The GHX-analysis included 12 optimisation variables and six non-linear constraints, which is obviously a challenging optimisation problem. Some of the optimisation variables in

Table 6 do not change monotonically with increasing total HX area. For instance, an increase in the evaporator length was expected when the total HX area was increased from 80 m^2 to 100 m^2 for propene. The decrease in the evaporator length for this case is due to the optimiser “getting stuck” in a local optimum in at least one of the two “total HX area” cases. However, the smooth monotonic curves of the net power output vs. total HX area in Fig. 6 indicate that the maximised net power

output is at least very close to the global maximum.

In this paper the GHC-analysis was applied to analyse different RC-systems at design conditions. However, the GHX-analysis can also be applied for "quasi steady-state" off-design analysis with, for instance, a heat source with time-dependent operating conditions. Such an analysis can be performed by optimising HX geometry for a given design condition and fixing this geometry in the off-design analysis.

5. Conclusions

Selection of fluid, cycle layout and component types are important issues when designing a Rankine cycle and the optimal outcome is very dependent on the target application. Thermodynamic analysis is a common methodology for screening multiple Rankine cycle options in terms of thermodynamic performance potential, but additional assumptions are required to estimate component sizes such as HX area. The GHX-analysis is presented as a more informative alternative method for screening or initial Rankine cycle analysis by introducing a generic heat exchanger (GHX) model. The GHX model does not represent a certain HX-type or even a manufacturable design, but applies fluid properties and a minimum amount of generic geometry parameters to estimate local heat transfer coefficients and pressure gradients. The GHX-analysis thus permits simultaneous optimization of process state points and the trade-off between overall heat transfer coefficient and pressure drop without relying on a certain HX-geometry concept. The GHX-analysis was demonstrated for analysing a single stage recuperated RC with different working fluids and HX sizes, and compared with pure thermodynamic approaches. The main conclusions drawn from this work are the following:

- Both thermodynamic- and GHX-analysis can be applied independently of the HX-type(s) under consideration. However, GHX-analysis provides a quantitative measure of HX size in terms of HX area, instead of the qualitative UA-value from the thermodynamic analysis.
- The optimal HX design predicted by the GHX-analysis (e.g. pressure drop and flow cross-sectional area) gives a "flying start" for designing heat exchangers for the target application.
- The trade-off between overall HTC and pressure drop is a compromise between exergy losses due to pressure drop and finite temperature difference between two fluids. The GHX-analysis demonstrates that the optimal trade-off is highly depended on the working fluid and on the total permitted HX area. Hence, the optimal pressure drop is an important parameter for determining the overall HTC, in addition to working fluid properties and flow-regimes.
- The present study focuses on presenting a methodology, rather than designing a Rankine cycle for a target application. However, it should be noted that the GHX-analysis is not limited to analysis at design operating conditions, but can also be applied to predict off-design behaviour in heat exchangers.

Declaration of Competing Interest

The authors declared that there is no conflict of interest.

Acknowledgement

The authors gratefully acknowledge the financial support from the Research Council of Norway (EnergiX grant no. 255016) for the COPRO project, and the user partners Equinor, Norway; Hydro Norway; Alcoa, Norway; GE Power Norway and FrioNordica, Norway.

Appendix A. Supplementary material

Supplementary data to this article can be found online at https://doi.org/10.1016/j.applthermaleng.2019.114566.

References

[1] S. Quoilin, et al., Techno-economic survey of Organic Rankine Cycle (ORC) systems, Renew. Sustain. Energy Rev. 22 (2013) 168–186.
[2] F. Tchanche, B.M. Pétrissans, G. Papadakis, Heat resources and organic Rankine cycle machines, Renew. Sustain. Energy Rev. 39 (2014) 1185–1199.
[3] M. Imran, et al., Recent research trends in organic Rankine cycle technology: A bibliometric approach, Renew. Sustain. Energy Rev. 81 (2018) 552–562.
[4] M. Astolfi, E. Martelli, L. Pierobon, Thermodynamic and technoeconomic optimization of Organic Rankine Cycle systems, Organic Rankine Cycle (ORC) Power Systems, Elsevier, 2017, pp. 173–249, , https://doi.org/10.1016/B978-0-08-100510-1.00007-7.
[5] K.H. Kim, H.J. Ko, K. Kim, Assessment of pinch point characteristics in heat exchangers and condensers of ammonia–water based power cycles, Appl. Energy 113 (2014) 970–981.
[6] J. Sarkar, Generalized pinch point design method of subcritical-supercritical organic Rankine cycle for maximum heat recovery, Energy 143 (Supplement C) (2018) 141–150.
[7] M. Chys, et al., Potential of zeotropic mixtures as working fluids in organic Rankine cycles, Energy 44 (1) (2012) 623–632.
[8] A. Schuster, S. Karellas, R. Aumann, Efficiency optimization potential in supercritical Organic Rankine Cycles, Energy 35 (2) (2010) 1033–1039.
[9] C. Vetter, H.-J. Wiemer, D. Kuhn, Comparison of sub- and supercritical Organic Rankine Cycles for power generation from low-temperature/low-enthalpy geothermal wells, considering specific net power output and efficiency, Appl. Therm. Eng. 51 (1) (2013) 871–879.
[10] R. Agromayor, L.O. Nord, Fluid selection and thermodynamic optimization of organic Rankine cycles for waste heat recovery applications, Energy Procedia 129 (Supplement C) (2017) 527–534.
[11] Y. Wu, Y. Zhu, L. Yu, Thermal and economic performance analysis of zeotropic mixtures for Organic Rankine Cycles, Appl. Therm. Eng. 96 (2016) 57–63.
[12] N.A. Lai, J. Fischer, Efficiencies of power flash cycles, Energy 44 (1) (2012) 1017–1027.
[13] H. Yu, D. Kim, T. Gundersen, A study of working fluids for Organic Rankine Cycles (ORCs) operating across and below ambient temperature to utilize Liquefied Natural Gas (LNG) cold energy, Energy 167 (2019) 730–739.
[14] J. Vivian, G. Manente, A. Lazzaretto, A general framework to select working fluid and configuration of ORCs for low-to-medium temperature heat sources, Appl. Energy 156 (2015) 727–746.
[15] Y.R. Li, et al., Effect of pinch point temperature difference on cost-effective performance of organic Rankine cycle, Int. J. Energy Res. 37 (15) (2013) 1952–1962.
[16] D. Maraver, et al., Systematic optimization of subcritical and transcritical organic Rankine cycles (ORCs) constrained by technical parameters in multiple applications, Appl. Energy 117 (2014) 11–29.
[17] A.A. Lakew, O. Bolland, Working fluids for low-temperature heat source, Appl. Therm. Eng. 30 (10) (2010) 1262–1268.
[18] J. Wang, M. Diao, K. Yue, Optimization on pinch point temperature difference of ORC system based on AHP-Entropy method, Energy 141 (2017) 97–107.
[19] H.-H. Zhu, K. Wang, Y.-L. He, Thermodynamic analysis and comparison for different direct-heated supercritical CO2 Brayton cycles integrated into a solar thermal power tower system, Energy 140 (2017) 144–157.
[20] Rohde, D., et al. Comparison of rankine cycle and trilateral flash cycle for power production from low temperature heat sources, in: Refrigeration Science and Technology, 2018.
[21] K. Braimakis, et al., Low grade waste heat recovery with subcritical and supercritical Organic Rankine Cycle based on natural refrigerants and their binary mixtures, Energy 88 (2015) 80–92.
[22] D. Walraven, B. Laenen, W. D'Haeseleer, Economic system optimization of air-cooled organic Rankine cycles powered by low-temperature geothermal heat sources, Energy 80 (2015) 104–113.
[23] D. Walraven, B. Laenen, W. D'haeseleer, Minimizing the levelized cost of electricity production from low-temperature geothermal heat sources with ORCs: Water or air cooled? Appl. Energy 142 (2015) 144–153.
[24] V.L. Le, et al., Thermodynamic and economic optimizations of a waste heat to power plant driven by a subcritical ORC (Organic Rankine Cycle) using pure or zeotropic working fluid, Energy 78 (Supplement C) (2014) 622–638.
[25] Y. Feng, et al., Thermoeconomic comparison between pure and mixture working fluids of organic Rankine cycles (ORCs) for low temperature waste heat recovery, Energy Convers. Manage. 106 (Supplement C) (2015) 859–872.
[26] S. Quoilin, et al., Thermo-economic optimization of waste heat recovery Organic Rankine Cycles, Appl. Therm. Eng. 31 (14) (2011) 2885–2893.
[27] S. Lecompte, et al., Part load based thermo-economic optimization of the Organic Rankine Cycle (ORC) applied to a combined heat and power (CHP) system, Appl. Energy 111 (2013) 871–881.
[28] F. Capra, E. Martelli, Numerical optimization of combined heat and power Organic Rankine Cycles – Part B: Simultaneous design & part-load optimization, Energy 90 (2015) 329–343.
[29] B. Dong, et al., Thermodynamic and economic analysis of zeotropic mixtures as working fluids in low temperature organic Rankine cycles, Appl. Therm. Eng. 132 (2018) 545–553.
[30] D. Walraven, B. Laenen, W. D'haeseleer, Comparison of shell-and-tube with plate heat exchangers for the use in low-temperature organic Rankine cycles, Energy Convers. Manage. 87 (2014) 227–237.
[31] H.T. Walnum, et al., Modelling and simulation of CO2 (carbon dioxide) bottoming cycles for offshore oil and gas installations at design and off-design conditions,

Energy 59 (2013) 513–520.
[32] D. Rohde, et al., Heat recovery from export gas compression: Analyzing power cycles with detailed heat exchanger models, Appl. Therm. Eng. 60 (1) (2013) 1–6.
[33] V. Gnielinski, New equations for heat and mass transfer in turbulent pipe and channel flow, Int. Chem. Eng. 16 (2) (1976) 359–368.
[34] W.N. Selander, Explicit formulas for the computation of friction factors in turbulent pipe flow. 1978: Chalk River, Ontario, Canada: Chalk River Nuclear Labs.
[35] L.D. Boyko, G.N. Kruzhilin, Heat transfer and hydraulic resistance during condensation of steam in a horizontal tube and in a bundle of tubes, Int. J. Heat Mass Transf. 10 (3) (1967) 361–373.
[36] D.L. Bennet, J.C. Chen, Forced convective boiling in vertical tubes for saturated pure components and binary mixtures, AIChE J. 26 (3) (1980) 454–461.
[37] L. Silver, Gas cooling with aqueous condensation, Trans. Inst. Chem. Eng. 25 (1947) 30–42.
[38] J.K.G. Bell, M. A., An approximate generalized design method for multicomponent/partial condensers. AIChE Symp. Ser., vol. 69, 1973, pp. 72–79.
[39] L. Friedel, Improved friction pressure drop correlations for horizontal and vertical two-phase pipe flow, vol. 18, 1979, pp. 485–491.
[40] E. Lemmon, M. Huber, M. M., NIST reference database 23: reference fluid thermodynamic and transport propeties-REFPROP, version 9.1, Standard Reference Data Propgram, 2013.
[41] K. Schittkowski, NLPQL: A fortran subroutine solving constrained nonlinear programming problems, Ann. Oper. Res. 5 (2) (1986) 485–500.